Lattice dynamics of hexagonal and cubic InN: Raman-scattering experiments and calculations

G. Kaczmarczyk,[a] A. Kaschner, S. Reich, A. Hoffmann, and C. Thomsen
Institut für Festkörperphysik, TU Berlin, 10623 Berlin, Germany

D. J. As, A. P. Lima,[b] D. Schikora, and K. Lischka
Universität/GH Paderborn, FB 6 Physik, 33098 Paderborn, Germany

R. Averbeck and H. Riechert
Infineon Technologies, Corporate Research, CPR 7, Otto Hahn Ring 6, 81730 München, Germany

(Received 13 September 1999; accepted for publication 16 February 2000)

We present results of first- and second-order Raman-scattering experiments on hexagonal and cubic InN covering the acoustic and optical phonon and overtone region. Using a modified valence-force model, we calculated the phonon dispersion curves and the density of states in both InN modifications. The observed Raman shifts agree well the calculated Γ-point frequencies and the corresponding overtone density of states. A tentative assignment to particular phonon branches is given. © *2000 American Institute of Physics.* [S0003-6951(00)03015-1]

The group-III nitrides (GaN and AlN) have become the focus of materials research because their large direct band gap makes them suitable for optoelectronic applications in the blue and ultraviolet spectral region. The energy of the band gap can be varied by mixing the nitrides to their ternary combinations. A key component for band-gap energies in the visible range is InN. For the implementation of the nitrides in optoelectronic devices, a detailed knowledge of their fundamental physical properties is necessary.

Raman spectroscopy has proven to be a powerful tool for the investigation of material properties such as doping concentration, defect identification, or crystal orientation, as well as in the study of the phonon dynamics in GaN.[1,2] The lattice dynamics of GaN and AlN have been investigated intensively,[3–7] while for InN only a few reports exist.[8–12] The energy of the observed phonons of InN is summarized in Table I. Dyck *et al.*[10] complemented the experimental results with calculations, where they predicted the frequency of the E_2 (low) mode to be at $104\,\mathrm{cm}^{-1}$. Recently, Inushima, Shiraishi, and Davydov[11] presented a complete spectrum with all six Raman-active modes, i.e., E_2 at 87 and 488, E_1(TO) at 476, A_1(TO) at 480, E_1(LO) at 570, and A_1(LO) at $580\,\mathrm{cm}^{-1}$. For cubic InN Tabata *et al.*[12] determined the frequencies of the TO at 457 and the LO at $588\,\mathrm{cm}^{-1}$.

Only a few calculations of the phonon frequencies of both InN modifications were published; in addition to Dyck *et al.*'s results on hexagonal InN, Tabata *et al.*[12] calculated the Γ-point frequencies of cubic InN. Bechstedt and Grille[13] reported the phonon-dispersion curves along the $\Gamma \rightarrow \mathrm{L}$ direction for the cubic modification from an *ab initio* calculation.

In this letter, we present second-order Raman spectra of both the hexagonal and cubic modifications of InN. We performed calculations of the dispersion curves of both modifications. The spectral region investigated contained the overtone of the acoustic as well as the optical phonons and their combinations. From the experiments, we determine the phonon energies at the Γ point and at the zone boundary of InN and compare the results with our calculations.

The samples investigated were an about 120-nm-thick layer of hexagonal InN grown on (0001) GaN and a 1-μm-thick layer of cubic InN grown on (001) GaAs by plasma-assisted molecular-beam epitaxy. To improve the quality of the InN layers, a buffer layer was grown on the substrate; InAs (300 nm) was used for the cubic InN layer and for hexagonal InN, a GaN (900 nm) layer.[14,15] The Raman-scattering experiments were carried out using a Dilor XY and a LABRAM spectrometer with a charge-coupled-device detector. The 488 nm line of an Ar^+/Kr^+ laser and the 632.8 nm line of a He–Ne laser were used for excitation. The scattered light was detected in backscattering geometry which corresponded to A_1(LO) and E_2 symmetry. Because of the small thickness of the InN layers, in-plane scattering, for which the A_1(TO) becomes Raman active, was not possible. All spectra are accurate to $\pm 1\,\mathrm{cm}^{-1}$.

InN exists in both the cubic and hexagonal modifications, which differ in the packing sequence only. Hexagonal InN grows in the wurtzite structure (point group C_{6v}) with four atoms per unit cell. For the $\mathbf{k}=0$ group, theory predicts the following set of optical modes: $\Gamma_{\mathrm{vib}}^{\mathrm{opt}} = A_1 + 2B_1 + E_1 + 2E_2$. Except for the silent B_1 modes all modes are Raman active. Cubic InN has a zinc-blende structure and belongs to the point group T_d with two atoms per unit cell, and thus six phonon branches. At $\mathbf{k}=0$ the optical modes have T_2 symmetry.

Figure 1(a) shows a room-temperature first-order Raman spectrum of the hexagonal InN layer. The upper curve was recorded in A_1+E_2 symmetry and the lower one in E_2 configuration. The most intense peaks are located at 88, 440, 464, 490, 542, 568, and $590\,\mathrm{cm}^{-1}$ and labeled according to their symmetry. The peak at $88\,\mathrm{cm}^{-1}$ of the E_2 (low) phonon overlaps with a plasma line of the He/Ne laser. In order to verify the E_2 character of this peak we measured both con-

[a]Electronic mail: geka@mail.physik.tu-berlin.de
[b]Present address: Walter Schottky Institut, TU München, Am Coulombwall, 85748 Garching, Germany.

TABLE I. Summary of the experimentally observed phonons of InN (cubic and hexagonal modifications). Experimental values (given in cm^{-1}) were taken from Refs. 9–12.

InN (hex)	Ref. 9	Ref. 10		Ref. 11	Present work		InN (cub)	Ref. 12	Present work	
		exp.	calc.		exp.	calc.			exp.	calc.
E_2 (low)			104	87	88	93				
B_1			270	200		202				
E_1 (TO)		475	472	476		470				
A_1 (TO)		446	440	480	440	443	TO	457	472	470
E_2 (high)	495	488	483	488	490	492				
B_1			530	540		568				
E_1 (LO)				570		605				
A_1 (LO)	596	574		580	590	589	LO	588	586	588

figurations (parallel and perpendicular) with $\lambda_{exc}=488\,nm$; the inset in Fig. 1(a) shows that the peak, within experimental error, is equally strong in both configurations, and thus indeed of E_2 symmetry. The energy of the E_2 phonons at 88 and 490 cm^{-1} is in good agreement with those reported by Inushima *et al.*[11] The position of the A_1 phonons is, however, different. Inushima *et al.*, in their spectra, show a very weak feature at 440 cm^{-1} near the feature that they assigned to the TO. Due to the better signal-to-noise ratio, this structure is more distinct in our spectrum and has clear A_1 symmetry, just as the mode at 590 cm^{-1} does. The TO is much smaller than the LO because it is actually forbidden in this scattering geometry. Imperfections in the lattice structure may make it appear in the spectra. In the GaN buffer layer the A_1(TO), also forbidden in a perfect crystal, and the E_2 (high) phonon modes are detected at 542 and 568 cm^{-1}. The origin of the peak at 464 cm^{-1} is currently not clear; in this frequency region the E_1 modes were observed in IR spectroscopy,[11] but are also forbidden for the scattering geometries accessible to us.

Several structures were observed in addition to the first-order phonons. In Fig. 1(b) the second-order Raman spectra are plotted. The low-frequency region, approximately 100–210 cm^{-1}, exhibits a broad feature with maxima at 110, 145, and 205 cm^{-1} with A_1 symmetry. This region is dominated by overtones of the acoustic phonons. The right part of Fig. 1(b) shows the high-frequency region of the spectrum. Apart from the first-order mode A_1(LO) of hexagonal GaN (736 cm^{-1}), weak additional features due to second-order processes in InN can be seen. In particular, we observed structures at 678, 1092, and 1188 cm^{-1}.

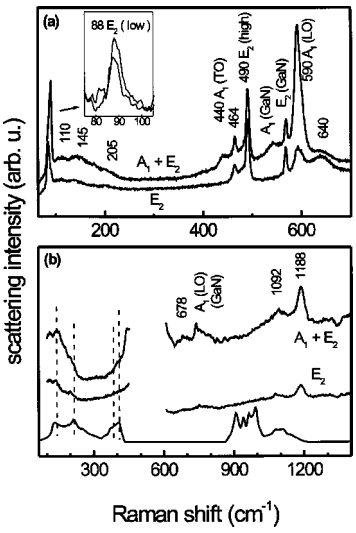

FIG. 1. First-order (a) and second-order (b) Raman spectra of hexagonal InN taken at room temperature for scattering geometries corresponding to A_1+E_2 and E_2 symmetries. The lowest trace in (b) shows the calculated density of states. The excitation wavelength was 632.8 nm (first order) and 488 nm (second order). The inset ($\lambda_{exc}=488$ nm) shows the E_2 (low) mode for both scattering configurations.

In order to assign these structures, we carried out calculations of the phonon-dispersion curves of hexagonal InN. Our model is based on the modified valence-force model of Keating[16] and Kane,[17] including up to the third-nearest-neighbor interactions as well as the Coulomb interaction. The anisotropy of hexagonal crystals was accounted for with a set of parameters describing interactions along and perpendicular to the c axis.[18] They were used to set up the dynamical matrix, the eigenvalues of which are the squares of vibrational frequencies. Figure 2 exhibits the calculated phonon-dispersioncurves of hexagonal InN and the corresponding density of states.

Comparing the calculated phonon-dispersion curves in the low-frequency region, we can assign the overtones of transverse-acoustic phonons. While the structure around 145 cm^{-1} can be attributed to acoustic phonons around the A point, the structure located at 205 cm^{-1} is presumably due to overtones of TA phonons either near the symmetry point K or M of the Brillouin zone. In contrast to Inushima *et al.*,[11] we interpret the weak structure around 200 cm^{-1} as second-order processes of the acoustic phonons and not as the B_1 (low) silent mode, which should be much too weak to be observed.

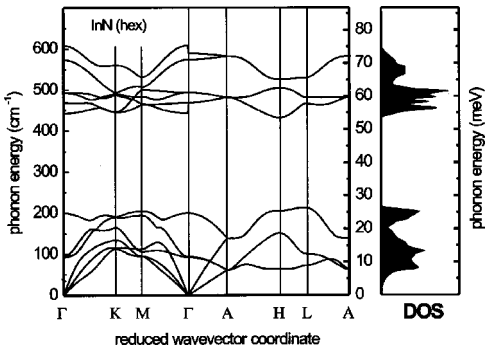

FIG. 2. Calculated phonon-dispersion curves of hexagonal InN and corresponding density of states.

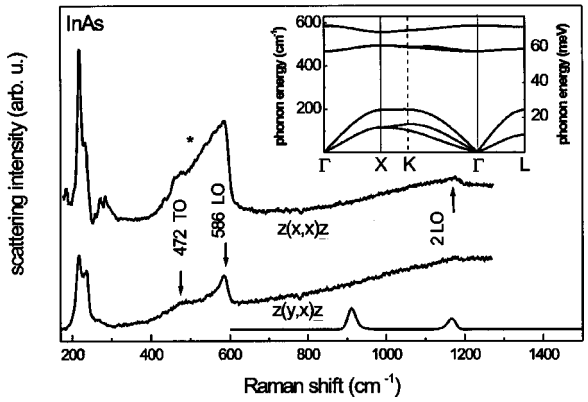

FIG. 3. First-order and second-order Raman spectra of cubic InN taken at room temperature for $z(x,x)\bar{z}$ and $z(y,x)\bar{z}$ configurations. The excitation wavelength was 632.8 nm, in resonance with the band gap of InN. The high intensity marked by * is caused by the second-order signal of InAs. The lowest curve shows the calculated density of states of the overtones. In the inset we present the calculated phonon dispersion curves of cubic InN.

The optical and acoustic combinations and the second-order optical structures lie in the high-frequency part of the spectrum between 600 and 1200 cm^{-1}. The structure at 678 cm^{-1}, from frequency considerations, can only be a combination of optical and acoustic phonons. We interpret the peak at 678 cm^{-1} with A_1 symmetry as additive combination of A_1(LO)+A_1(LA) near the symmetry point K or M of the Brillouin zone. Between 850 and 1200 cm^{-1} we observe an increase in intensity in both scattering geometries. These structures coincide with the calculated overtones although they do not appear as pronounced in the calculation. The maxima in this band are located at 1092 and 1188 cm^{-1}. The peak at 1188 cm^{-1} is attributed to an overtone of the highest LO branch, the cutoff at 1220 cm^{-1} corresponds to twice the zone-center A_1(LO) mode frequency.

Figure 3 shows room-temperature first-order Raman spectra of cubic InN in the range from 200 to 700 cm^{-1} excited at 632.8 nm, in resonance with the band gap of InN. We observe structures at 218, 237, 470, and 586 cm^{-1}. The InN TO and LO modes are found at 470 and 586 cm^{-1}. Because of the buffer layer we see phonons of InAs in addition to those of cubic InN; the InAs TO and LO phonons are at 217 and 238 cm^{-1}, respectively.[19] While the LO frequency of InN agrees with the values reported by Tabata *et al.*,[12] who excited their spectra above-band gap (λ_{exc} = 514.5 nm), they assigned a feature at 458 cm^{-1} to the TO phonon of cubic InN. The nonresonant spectra of Ref. 12 are, however, similar to the second-order spectra of InAs,[19] making it difficult to assign the TO of InN uniquely. Because of the resonant excitation, we observe the first-order features of InN much more strongly (intensity $LO_{InN}/TO_{InAs}=0.36$) relative to those of InAs than when exciting at 514.5 nm ($LO_{InN}/TO_{InAs}=0.04$). In addition, we suppressed the second-order InAs contribution to the spectrum by using crossed polarizations. Rotating the sample by 180° in steps of 10° we find the expected angular dependence of T_2 symmetry modes in a cubic material for both peaks at 470 and 586 cm^{-1}; the intensity has two maxima versus angle separated by approximately 90°. The spectra shown in Fig. 3 were taken at an angle with the maximum intensity of the InN features in crossed polarizations corresponding to electric-field vectors parallel to the crystallographic axes.

Based on our experimental data we performed a calculation of the phonon-dispersion curves of cubic InN, shown in the inset of the Fig. 3. For the iterative fit procedure of the cubic dispersion curves we used the Kane parameters of cubic GaN and our LO(Γ) and TO(Γ) phonon frequencies of InN. Due to the large difference between In and Ga atoms, all phonon branches are shifted to lower energies. The propagation of the phonon branches along the Γ→L direction agree well with those reported by Bechstedt and Grille,[13] and they agree with the calculated curves for hexagonal InN. The TA and LA branches are backfolded into the E_2 (low) and B_1 (low) branches, respectively, corresponding to the transition from cubic to hexagonal symmetry. Similar backfolding occurs for the cubic LO and TO into hexagonal B_1 (high) and E_2 (high).

To summarize, we presented first- and second-order Raman scattering results of hexagonal and cubic InN. Most of the first-order phonon frequencies agree with the literature. We compared the experimentally observed first- and second-order phonon energies to the phonon-dispersion curves calculated by a valence-force model by Kane and find good agreement.

This work was partially supported by the Deutsche Forschungsgemeinschaft, Volkswagenstiftung. One of the authors (A.K.) acknowledges an Ernst von Siemens fellowship.

[1] A. Kaschner, H. Siegle, G. Kaczmarczyk, M. Strassburg, A. Hoffmann, C. Thomsen, U. Birkle, S. Einfeld, and D. Hommel, Appl. Phys. Lett. **74**, 3281 (1999).
[2] H. Siegle, L. Eckey, A. Hoffmann, C. Thomsen, B. K. Meyer, D. Schikora, M. Hankeln, and K. Lischka, Solid State Commun. **96**, 943 (1995).
[3] P. Perlin, C. J. Carrilon, J. P. Itie, A. S. Miguel, I. Grzegory, and A. Polian, Phys. Rev. B **45**, 83 (1992).
[4] K. Karch and F. Bechstedt, Phys. Rev. B **56**, 7404 (1997).
[5] H. Siegle, G. Kaczmarczyk, L. Filippidis, A. P. Litvinchuk, A. Hoffmann, and C. Thomsen, Phys. Rev. B **55**, 7000 (1997).
[6] K. Karch, J.-M. Wagner, and F. Bechstedt, Phys. Rev. B **57**, 7043 (1998).
[7] V. Yu. Davydov, Yu. E. Kitaev, I. N. Goncharuk, A. N. Smirnow, J. Graul, O. Semchinova, D. Uffmann, M. B. Smirnov, A. P. Mirgorodsky, and R. A. Evarestov, Phys. Rev. B **58**, 12899 (1998).
[8] T. Inushima, T. Yaguchi, A. Nagase, A. Iso, and T. Shiraishi, Inst. Phys. Conf. Ser. **142**, 971 (1995).
[9] H. Kwon, Y. Lee, O. Miki, H. Yamano, and A. Yoshida, Appl. Phys. Lett. **69**, 937 (1996).
[10] J. S. Dyck, K. Kash, K. Kim, W. R. L. Lambrecht, C. C. Hayman, A. Argoitia, M. T. Grossner, W. L. Zhou, and J. C. Angus, Mater. Res. Soc. Symp. Proc. **482**, 549 (1998).
[11] T. Inushima, T. Shiraishi, and V. Yu. Davydov, Solid State Commun. **110**, 491 (1999).
[12] A. Tabata, A. P. Lima, L. K. Teles, L. M. R. Scolfaro, J. R. Leite, V. Lemos, B. Schöttker, T. Frey, D. Schikora, and K. Lischka, Appl. Phys. Lett. **74**, 362 (1999).
[13] F. Bechstedt and H. Grille, Phys. Status Solidi B **216**, 761 (1999).
[14] A. P. Lima, A. Tabata, J. R. Leite, S. Kaiser, D. Schikora, B. Schröttker, T. Frey, D. J. As, and K. Lischka, J. Cryst. Growth **201-202**, 396 (1999).
[15] R. Averbeck and H. Riechert, Phys. Status Solidi A **176**, 301 (1999).
[16] P. N. Keating, Phys. Rev. **145**, 637 (1966).
[17] E. O. Kane, Phys. Rev. B **31**, 7865 (1985).
[18] C. Göbel, C. Schrepel, U. Scherz, P. Thurian, G. Kaczmarczyk, and A. Hoffmann, Mater. Sci. Forum **258-263**, 1173 (1997).
[19] R. Carles, N. Saint-Cricq, J. B. Renucci, M. A. Renucci, and A. Zwick, Phys. Rev. B **22**, 4804 (1980).